Journal of Applied Physics

Influence of annealing atmosphere on formation of electrically-active defects in rutile TiO_2

Cite as: J. Appl. Phys. **123**, 161572 (2018); https://doi.org/10.1063/1.5011136
Submitted: 30 October 2017 . Accepted: 13 December 2017 . Published Online: 23 January 2018

C. Zimmermann, J. Bonkerud, F. Herklotz, T. N. Sky, A. Hupfer, E. Monakhov, B. G. Svensson, and L. Vines

ARTICLES YOU MAY BE INTERESTED IN

Tutorial: Novel properties of defects in semiconductors revealed by their vibrational spectra
Journal of Applied Physics **123**, 161561 (2018); https://doi.org/10.1063/1.5011036

Tutorial: Junction spectroscopy techniques and deep-level defects in semiconductors
Journal of Applied Physics **123**, 161559 (2018); https://doi.org/10.1063/1.5011327

Iron and intrinsic deep level states in Ga_2O_3
Applied Physics Letters **112**, 042104 (2018); https://doi.org/10.1063/1.5020134

AIP Publishing

© 2018 Author(s).

JOURNAL OF APPLIED PHYSICS 123, 161572 (2018)

Influence of annealing atmosphere on formation of electrically-active defects in rutile TiO_2

C. Zimmermann,[1] J. Bonkerud,[1] F. Herklotz,[2] T. N. Sky,[1] A. Hupfer,[1] E. Monakhov,[1] B. G. Svensson,[1] and L. Vines[1]
[1]*Physics Department/Centre for Materials Science and Nanotechnology, University of Oslo, P.O. Box 1048, Blindern, Oslo N-0316, Norway*
[2]*Department of Physics, Freie Universität Berlin, 14195 Berlin, Germany*

(Received 30 October 2017; accepted 13 December 2017; published online 23 January 2018)

Electronic states in the upper part of the bandgap of reduced and/or hydrogenated *n*-type rutile TiO_2 single crystals have been studied by means of thermal admittance and deep-level transient spectroscopy measurements. The studies were performed at sample temperatures between 28 and 300 K. The results reveal limited charge carrier freeze-out even at 28 K and evidence the existence of dominant shallow donors with ionization energies below 25 meV. Interstitial atomic hydrogen is considered to be a major contributor to these shallow donors, substantiated by infrared absorption measurements. Three defect energy levels with positions of about 70 meV, 95 meV, and 120 meV below the conduction band edge occur in all the studied samples, irrespective of the sample production batch and the post-growth heat treatment used. The origin of these levels is discussed in terms of electron polarons, intrinsic point defects, and/or common residual impurities, where especially interstitial titanium atoms, oxygen vacancies, and complexes involving Al atoms appear as likely candidates. In contrast, no common deep-level defect, exhibiting a charge state transition in the 200–700 meV range below the conduction band edge, is found in different samples. This may possibly indicate a strong influence on deep-level defects by the post-growth heat treatments employed. *Published by AIP Publishing.* https://doi.org/10.1063/1.5011136

I. INTRODUCTION

Titanium dioxide (TiO_2) in its rutile form has gained considerable attention for its photocatalytic properties[1–3] or as part of solar cells.[4,5] However, the bandgap of rutile TiO_2 is approximately 3.2 eV,[6] which is too wide for utilizing the solar spectrum efficiently.[6] Recently, reduced and/or hydrogenated TiO_2 has received increasing interest because it exhibits stronger absorption in the visible/infrared wavelength regime than virgin rutile TiO_2.[7,8] However, the understanding of intrinsic and impurity-related defects in this material is not fully developed to date, but it is of key importance in virtually all of its applications.

Reduced and/or hydrogenated rutile TiO_2 exhibits *n*-type conductivity,[9–13] but the nature of the main donor(s) is still under debate even after decades of research. The oxygen vacancy (V_O), titanium interstitial (Ti_i), and hydrogen on an interstitial site (H_i) are considered to be potential sources of *n*-type doping.[10,11,14–19] However, the properties of these donors remain elusive and controversial. The question which of these defects are dominant might furthermore strongly depend on the actual sample treatment.[19] Importantly, hydrogen could be present in significant concentrations also in samples which were not intentionally hydrogenated.[18]

The identification of defects in rutile TiO_2 is particularly challenging as the energy scheme of the defect levels may be influenced by polaronic effects.[19–29] First, this makes the theoretical description of defects in rutile TiO_2 exceptionally challenging.[19,24] Second, polaronic effects can also lead to different defects having similar experimental signatures as electrons are trapped at similar Ti sites no matter which defect they actually originate from.[19] Another consequence of the polaronic effects is that techniques which probe thermal or optical transition energies will yield significantly different values for the same defect. Hence, they cannot directly be used complementarily in identifying defects.[19,20,23,24]

This can, for example, be observed in the case of H_i: Conductivity, transport, electron paramagnetic resonance, and infrared absorption measurements report on a shallow donor level with thermal transition energies of several meV,[10,11,25,30–32] while absorption data indicate optical transition energies of around 1–2 eV.[8,28,32,33]

Another prominent example is V_O. Some experiments indicate that V_O is a shallow donor in rutile TiO_2, responsible for the *n*-type conductivity observed in samples annealed at low oxygen partial pressure,[13,14,34] while other studies report V_O-related deep states.[35,36] This controversy concerning V_O is further complicated by the results of *ab-initio* calculations, as different studies strongly disagree on whether V_O induces shallow effective mass-like states or deep donor levels.[23,37–40]

Space-charge spectroscopic techniques such as thermal admittance spectroscopy (TAS),[41,42] deep-level transient spectroscopy (DLTS),[43] and thermally stimulated current spectroscopy (TSC)[44] probe thermal transition energies of electrically active defects. So far, only very few studies have been reported in the literature, where TAS,[36] DLTS,[35] and TSC[45,46] are applied to gain insights into defect properties of rutile TiO_2. Various defect levels between 130 meV and 870 meV below the conduction band edge have been reported; however, the identity of the associated defects remains unknown.

The scarcity of reports on space-charge spectroscopy performed on rutile TiO_2 is partially related to the difficulty in forming rectifying junctions.[35,47] However, recent progress, see e.g., Ref. 48, shows promising results for Schottky contacts of sufficient quality to pursue TAS and DLTS studies on rutile TiO_2.

In this work, we report on electrically active defects observed by TAS and DLTS measurements on rutile TiO_2 single crystals subjected to different reducing and/or hydrogenating heat-treatments. Our results show that techniques such as TAS and DLTS are highly applicable for systematic studies of electrically active defects in non-stoichiometric rutile TiO_2.

II. EXPERIMENTAL

The samples used in the present study were (001)-oriented rutile TiO_2 single crystals grown by the float zone method and were purchased from MTI Corporation. The samples were acquired at different occasions and represent several different production batches. The as-received single crystals were colorless and semi-insulating, reflected by a resistivity of $>10^7\ \Omega$ cm. After cutting into $5 \times 5\ mm^2$-sized samples, the crystals were cleaned in an ultrasonic bath with acetone, isopropanol, and deionized water for 5 min each. Afterwards, the samples were subjected to one of the three following heat treatments (annealings) using a tube furnace:

1. Annealing in forming gas flow ($N_2 + H_2$ with $[H_2]/[N_2] \approx 1/9$, where the square brackets denote the concentration) at temperatures between 500 °C and 600 °C for 35–75 min. (*forming gas annealing*)
2. Annealing in closed ampules filled with H_2 gas (0.5 bar at room temperature) for 20 min or 40 min. The ampules were evacuated with a roughing pump before filling with H_2. (*H_2 gas annealing*)
3. Annealing in N_2 flow at temperatures between 980 °C and 1250 °C for 1.25–25 h. (*N_2 gas annealing*)

The samples were always put into the furnace when the desired annealing temperature T_{anneal} was reached. After the heat treatment, the samples were cooled-down without force in the cold furnace zone while maintaining the gas flow. Subsequently, the annealed crystals were cleaned again using the afore-mentioned procedure and further boiled in H_2O_2 (40%) for 1–3 min. This treatment is commonly used for the preparation of Schottky diodes on ZnO and has proven to lead to highly rectifying diodes.[49]

Between 10 and 15 Pd contacts with a thickness in the range of ~150–200 nm were deposited onto the samples via electron beam evaporation, using a Si shadow mask with pad areas of 0.7×10^{-3} to 4.2×10^{-3} cm^2. Eutectic InGa was used as Ohmic back contact.

Secondary ion mass spectrometry (SIMS) measurements were performed using a Cameca IMS 7f instrument with a primary beam of 10 keV O_2^+ ions. Rutile TiO_2 samples implanted with Cr, Al, or Si were used as references to obtain absolute concentration values. For other residual elements, relative concentrations were determined. A constant erosion rate was assumed for depth-calibration, where the crater depths were measured using a surface Stylus Profilometer.

Fourier transform infrared (FTIR) absorbance spectra were recorded with a Bruker IFS125 HR spectrometer equipped with a globar or tungsten light source, a KBr or CaF_2 beam splitter, and an InSb detector. Measurements were performed with a spectral resolution of 0.5 cm^{-1} and at a sample temperature of 27 K. Unpolarized light was used with the wave vector, $\vec{k}$, directed perpendicular to the $\vec{c}$-axis of the samples.

The current-voltage (IV) and capacitance-voltage (CV) measurements were carried out under dark conditions at room temperature using a Keithley 6487 unit and an Agilent 4284A LCR meter, respectively.

DLTS was conducted using a refined version of the setup described elsewhere.[50] In short, the setup utilizes a Boonton 7200 capacitance meter and a closed-cycle He cryostat. During measurements, reverse bias voltages between –4 V and –3 V were applied. Filling pulses with an amplitude of 2 V to 4 V and a duration of 50 ms were employed. The DLTS signal was extracted from the acquired capacitance-versus-time transients using a lock-in weighting function[51] with six different rate windows in the range of $(20\ ms)^{-1}$ to $(640\ ms)^{-1}$. A delay time of 5 ms and a temperature resolution of 1 K were used. Measurements were performed both during heat-up and cool-down.

TAS measurements were conducted with a temperature resolution of 1 K during heat-up and cool-down using an Agilent 4284A LCR meter at probe frequencies f_{meas} between 10 kHz and 1 MHz. Further details about the setup used can be found in Ref. 52.

III. RESULTS

SIMS measurements were performed in order to monitor selected relevant impurities in the heat-treated samples. Cr and Li, Al, and Si are present in significant concentrations, where the relative concentrations vary by at least an order of magnitude between different samples for Cr (10^{16}–10^{17} cm^{-3}), Al (10^{16}–10^{17} cm^{-3}), and Li ($\leq 10^{16}$ cm^{-3}), whilst lower variations are found for Si (10^{17} cm^{-3}).

FTIR measurements were undertaken to determine the concentration of interstitial hydrogen (H_i) from its O–H vibrational mode at ~3290 cm^{-1}.[30,53] The as-received TiO_2 samples reveal a H_i concentration in the range of $1–3 \times 10^{16}$ cm^{-3}. The heat treatments result in an increase of $[H_i]$. For the N_2 gas annealed samples, $[H_i]$ increases to about 5×10^{17} cm^{-3}. Substantially, more H_i is observed in the case of annealing in H_2 gas or forming gas. In both cases, precise quantitative measurements are prevented because of the high $[H_i]$, leading to saturation of the O–H vibrational mode in the FTIR absorbance spectra.

Generally, different Pd/TiO_2/InGa junctions on the same TiO_2 sample display different IV characteristics, especially in terms of rectification. This indicates an inhomogeneity of the as-received samples unveiled by the applied annealing procedure. For some diodes, rectifications of up to six orders of magnitude in current can be found when the applied voltage V is varied between –4 V and 4 V. In Fig. 1, examples of

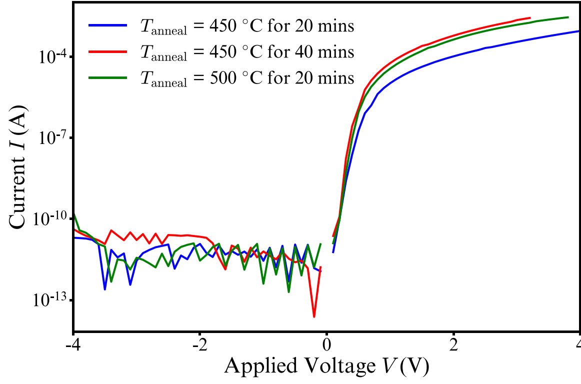

FIG. 1. IV curves of Pd Schottky contacts on H_2 gas annealed TiO_2 single crystals.

such IV curves are shown for H_2 gas annealed samples. In general, similar results are obtained independently of the specific annealing procedure used.

In Fig. 2, the results of CV measurements using different probe frequencies (4 kHz–1 MHz) are shown for two Pd/TiO_2/InGa junctions by depicting $1/C^2$ versus V. Two equivalent circuits consisting of only one resistance and capacitance were assumed to deduce the capacitance of the junctions (see also the inset of Fig. 2): (i) Capacitance C_P parallel to a resistance R_P (solid lines and left inset) and (ii) Capacitance C_S and a resistance R_S in series (dashed lines and right inset).

According to the depletion approximation, the depletion layer capacitance C_d of a Schottky junction on an n-type semiconductor is given by[54]

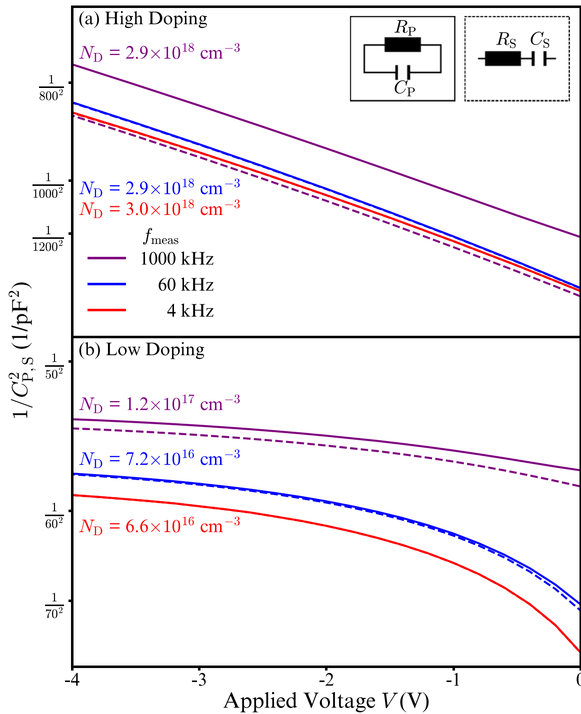

FIG. 2. Frequency-dependent $1/C^2_{P,S}$ - V plots for Pd Schottky contacts on forming gas annealed TiO_2 crystals. An equivalent circuit with the depletion layer capacitance C_d either in parallel (solid lines and left inset) or in series (dashed lines and right inset) with a resistance has been assumed.

$$C_d = \sqrt{\frac{A^2 \epsilon_0 \epsilon_r e N_D}{2(V_{bi} + V_{bias})}}. \tag{1}$$

Here, A denotes the junction area, ϵ_0 the vacuum permittivity, ϵ_r the static dielectric constant, e the elementary charge, N_D the donor concentration, V_{bi} the built-in voltage, and V_{bias} the applied bias voltage. A static dielectric constant ϵ_r of 100 was assumed.[10–12,55,56] For a uniform donor concentration, one expects a straight line for $1/C_d^2$ versus V,[54] which holds reasonably well for the highly doped sample in Fig. 2(a). From the slope of the curves, we obtain a donor concentration N_D of about $3 \times 10^{18}\,cm^{-3}$. For high reverse bias voltages and the highest probe frequency employed (1 MHz), a linear behavior is also observed for the low-doped sample [see Fig. 2(b)]. From the corresponding slope, a donor concentration N_D of about $1 \times 10^{17}\,cm^{-3}$ is obtained. For low reverse bias voltages and especially low probe frequencies, pronounced deviations from a linear dependence occur as will be commented on in the discussion Sec. IV A.

A. Thermal admittance spectroscopy

In TAS, the capacitance C and conductance G of a rectifying junction are determined as a function of sample temperature T and probe frequency f_{meas}[41,42] by assuming an appropriate equivalent circuit for the junction.[57] Here, a series circuit was assumed and the measured capacitance is denoted as C_S for series capacitance [see also the right inset of Fig. 2(a)].

When crossed by the Fermi level, shallow defect levels being present in the junction give rise to inflection points T_{inf} in the C–T spectra[41,42,58] and can be used to determine the activation energy (enthalpy) $E_A = E_C - E_D$ (E_C = conduction band edge and E_D = defect level position) of shallow states using[42,54]

$$\frac{2\pi f_{meas}}{T_{inf}^2} \sim \exp\left(-\frac{E_A}{k_b T_{inf}}\right), \tag{2}$$

where k_b denotes the Boltzmann constant.

Figure 3 shows representative TAS spectra obtained on four different Pd/TiO_2/InGa junctions. The corresponding TiO_2 samples were forming gas annealed (a) and (b), H_2 gas annealed (c), and N_2 gas annealed (d). Several inflection points in the C_S–T plots are revealed, which correspond to electron states being present in TiO_2. The values of T_{inf} to be used in Eq. (2) were extracted from the local maxima positions in the derivative spectra dC_S/dT[58] [see the example in the inset of Fig. 3(b)].

All the investigated forming gas annealed samples [see Figs. 3(a) and 3(b)] show the electron levels labeled $D_{2,FG}$ and $D_{3,FG}$. $D_{4,FG}$ is only present in some samples in sufficient concentrations to be detected by TAS. The levels labeled $D_{1,H}$, $D_{2,H}$, and $D_{3,H}$ are seen for all the investigated samples annealed in H_2 gas [see Fig. 3(c)]. For all the investigated samples annealed in N_2 gas, the levels $D_{2,N}$ and $D_{3,N}$ are observed, while $D_{4,N}$ is only detected in a few samples. $D_{1,FG}$, $D_{1,H}$, and $D_{1,N}$ can only be resolved at very low temperatures.

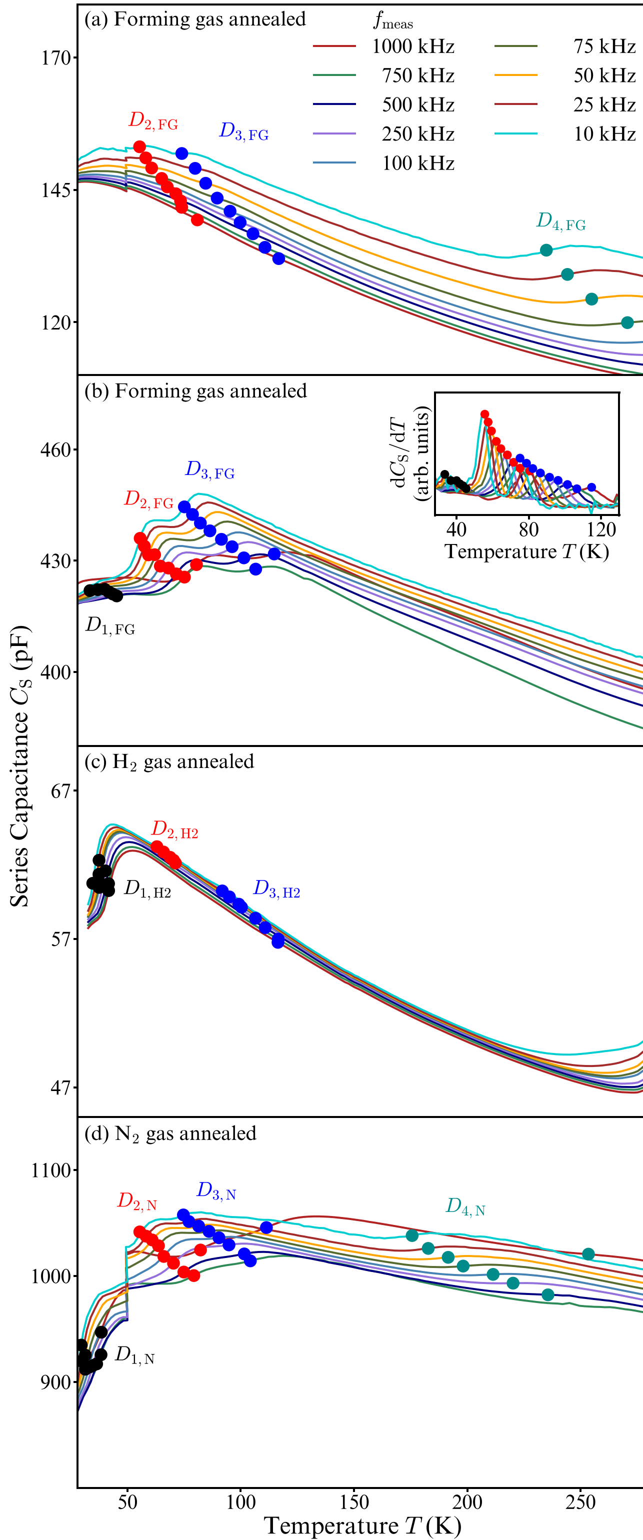

FIG. 3. C_S - T plots for four different $Pd/TiO_2/InGa$ junctions. The inset in (b) shows dC_S/dT over T, which was used to determine T_{inf} [see Eq. (2)].

By comparing the value pairs (T_{inf}, f_{meas}) for the electron levels observed in samples subjected to different heat-treatments, it is found that $D_{2,FG}$ and $D_{2,N}$, as well as $D_{3,FG}$ and $D_{3,N}$, respectively, can arise from the same electron levels.

Figure 4 displays Arrhenius plots obtained from the TAS spectra shown in Fig. 3 according to Eq. (2). Linear least-squares fits, represented by solid lines in Fig. 4, have been used to determine E_A. In Table I, the obtained activation energy values of the observed electron levels are summarized.

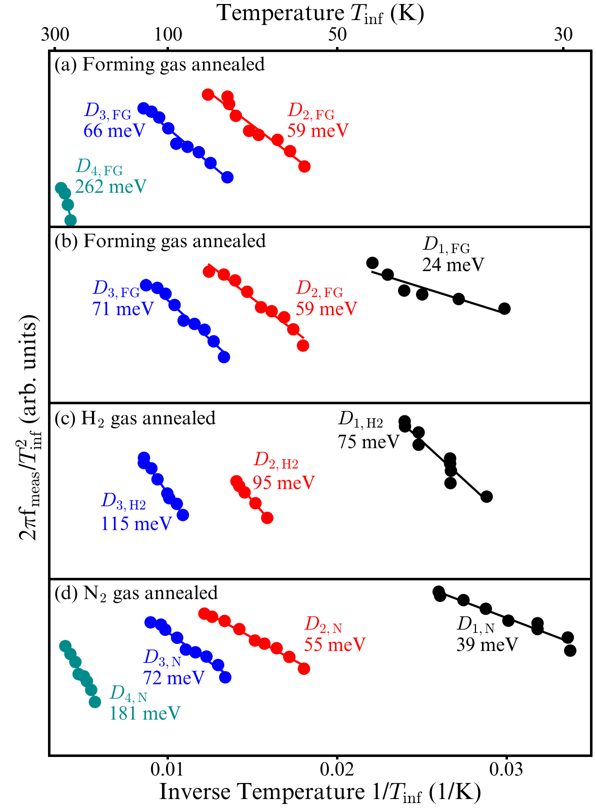

FIG. 4. Arrhenius plots derived from the C_S-T curves shown in Fig. 3 using Eq. (2).

B. Deep-level transient spectroscopy

DLTS was used to probe deep electron traps in heat-treated TiO_2 samples. The trap concentration N_T was deduced assuming a uniform and sufficiently low ($\leq 0.1 N_D$) defect distribution, where[43,54]

$$N_T = 2\frac{\Delta C}{C_{rb}} N_D. \quad (3)$$

Here, ΔC is determined from the measured capacitance transients,[43,51,54] while C_{rb} is the capacitance measured at the

TABLE I. Overview of thermal activation energies E_A determined by TAS on $Pd/TiO_2/InGa$ junctions. Subscript FG: forming gas annealing, N: N_2 gas annealing, and H2: H_2 gas annealing. The intervals stated take into account the fitting errors and the spread across the surface of the samples measured.

Forming gas annealed		H_2 gas annealed		N_2 gas annealed	
Defect level	E_A (meV)	Defect level	E_A (meV)	Defect level	E_A (meV)
$D_{1,FG}$	[19, 29]	$D_{1,H2}$	[67, 84]	$D_{1,N}$	[35, 42]
$D_{2,FG}$	[54, 65]	$D_{2,H2}$	[92, 98]	$D_{2,N}$	[53, 57]
$D_{3,FG}$	[62, 75]			$D_{4,N}$	[169, 192]
$D_{4,FG}$	[206, 318]				

quiescent reverse bias voltage. N_D is derived from CV measurements.[54]

For each DLTS rate window, the peak in ΔC occurs at a different T_{max}. Using the following relation for the electron emission rate e_n at the DLTS peak maximum[54]

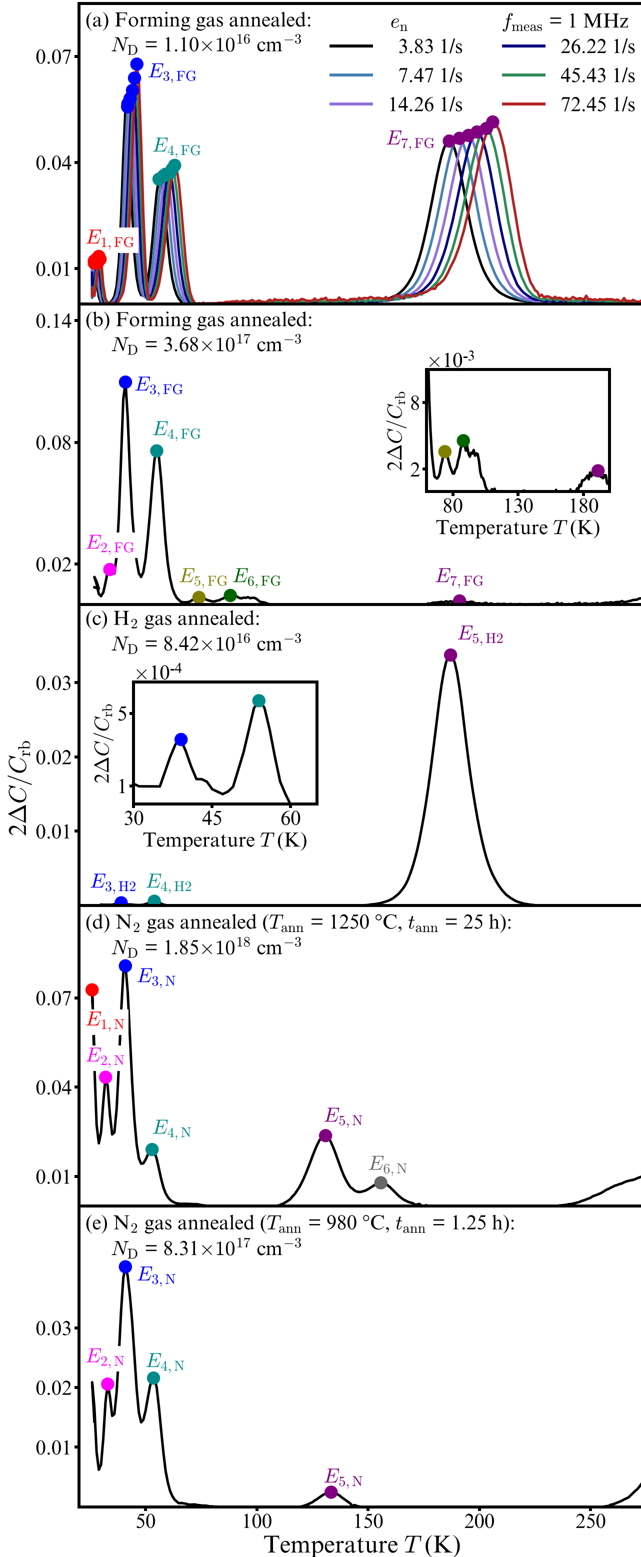

FIG. 5. DLTS results for five different $Pd/TiO_2/InGa$ junctions. In (a), results for the six rate windows used for obtaining Arrhenius plots are shown. In (b)–(e), only the results for the longest rate window are displayed ($e_n = 3.83\,s^{-1}$ at the peak maximum).

$$\frac{e_n}{T_{max}^2} = \beta \sigma_a \exp\left(-\frac{E_A}{k_b T_{max}}\right), \tag{4}$$

the apparent capture cross-section σ_a and the thermal activation energy E_A for the deep-level defect can be determined. β is a material-specific constant and is given by[43,54]

$$\beta = 2\sqrt{3}\left(\frac{2\pi}{h^2}\right)^{3/2} k_b^2 m_e^*. \tag{5}$$

Here, m_e^* denotes the effective electron mass in TiO_2, while h is the Planck constant. There is quite a spread in values reported for m_e^*.[11,34,59–64] In this study, a value of ten-times the free electron mass m_e is assumed.

Figure 5 displays exemplary DLTS spectra measured on $Pd/TiO_2/InGa$ junctions. Figures 5(a) and 5(b) show the results for forming gas annealed samples, where seven different defect levels are observed. The levels labeled $E_{3,FG}$ and $E_{4,FG}$ are present in all samples irrespective of the annealing conditions used (duration or temperature) and the specific production batch from which the TiO_2 single crystals originated. $E_{1,FG}$ appears at very low temperatures and was not resolved for all the measurements shown here. The levels $E_{2,FG}$, $E_{5,FG}$, $E_{6,FG}$, and $E_{7,FG}$ occur occasionally and were not observed in all the investigated samples.

In Fig. 5(c), a DLTS spectrum of a H_2 gas annealed sample is shown. Different annealing durations and/or temperatures lead to qualitatively similar DLTS spectra with similar levels being present and $E_{5,H2}$ as the dominant one. All the investigated samples originated from the same production batch.

Figures 5(d) and 5(e) show DLTS results for the N_2 gas annealed samples. The samples originated from the same production batch but were subjected to different annealing durations and temperatures. The levels $E_{2,N}$, $E_{3,N}$, $E_{4,N}$, and $E_{5,N}$ are observed in all the samples, whereas $E_{6,N}$ is only present in samples annealed at high temperatures and for long durations. The level $E_{1,N}$ is very shallow and can only be resolved fully at low temperatures using short rate windows.

When comparing the (T_{max}, e_n) pairs for the observed defect levels across samples subjected to different heat-treatments, it can be found that the following defect levels may have the same origin: $E_{2,N}$ and $E_{2,FG}$, $E_{3,N}$, $E_{3,FG}$, and $E_{3,H2}$, and $E_{4,FG}$, $E_{4,N}$, and $E_{4,H2}$.

In Table II, an overview of the observed defect levels and their activation energy values, as well as apparent capture cross sections, is given. Due to the ambiguity concerning the value of the effective electron mass m_e^*, only orders of magnitude values are stated for σ_a.

IV. DISCUSSION

A. Experimental remarks

Generally, the $Pd/TiO_2/InGa$ junctions display high rectification (see Fig. 1) as required for accurate space-charge spectroscopy measurements. In the case of highly doped samples, the CV characteristics resemble those expected for a depletion layer capacitance under uniform doping [see the linear $1/C^2$ - V dependency in Fig. 2(a)]. However,

TABLE II. Overview of thermal activation energies E_A and apparent capture cross sections σ_a determined using DLTS on Pd/TiO_2/InGa junctions. Subscript FG: forming gas annealing, N: N_2 gas annealing, and H2: H_2 gas annealing. The intervals stated for E_A take into account fitting errors and the scatter between the measured samples. The values stated for σ_a take only into account the scatter across the surface of the samples because of the large uncertainty.

Forming gas annealed			H_2 gas annealed			N_2 gas annealed		
Defect level	E_A (meV)	σ_a (cm^2)	Defect level	E_A (meV)	σ_a (cm^2)	Defect level	E_A (meV)	σ_a (cm^2)
$E_{1,FG}$	[57, 76]	10^{-13}	$E_{1,H2}$	[49, 96]	10^{-11}	$E_{2,N}$	[63, 93]	[10^{-15}, 10^{-12}]
$E_{2,FG}$	[69, 96]	[10^{-14}, 10^{-12}]	$E_{3,H2}$	[81, 104]	10^{-14}	$E_{1,N}$	[82, 99]	10^{-12}
$E_{3,FG}$	[87, 111]	[10^{-15}, 10^{-13}]	$E_{4,H2}$	[92, 144]	[10^{-16}, 10^{-14}]	$E_{3,N}$	[86, 109]	[10^{-15}, 10^{-13}]
$E_{6,FG}$	[104, 114]	10^{-20}	$E_{5,H2}$	[446, 471]	[10^{-15}, 10^{-14}]	$E_{4,N}$	[110, 123]	10^{-15}
$E_{4,FG}$	[111, 132]	[10^{-15}, 10^{-14}]				$E_{5,N}$	[273, 313]	[10^{-16},10^{-15}]
$E_{5,FG}$	[204, 218]	10^{-12}				$E_{6,N}$	[365, 395]	[10^{-15}, 10^{-14}]
$E_{7,FG}$	[424, 630]	[10^{-14}, 10^{-13}]						

deviations from this behavior are evident for low doped samples [see Fig. 2(b)]. These deviations can be caused by a non-uniform doping concentration, a highly compensated interfacial layer being present between the metal contact(s) and TiO_2,[47,65–67] a high density of deep defect levels not responding fully to the probe frequency,[68] or high series resistance.[69,70]

Our set of data indicates that several of these causes contribute to the recorded CV characteristics, especially high series resistance and the presence of a highly compensated interfacial layer. We found that their relative contribution depends on the sample and its particular treatment. By using comparatively small contact areas, the effect of the high series resistance can be minimized,[69,70] and a detailed analysis of the CV characteristics and barrier heights of the Schottky junctions used in this work can be found in Ref. 48.

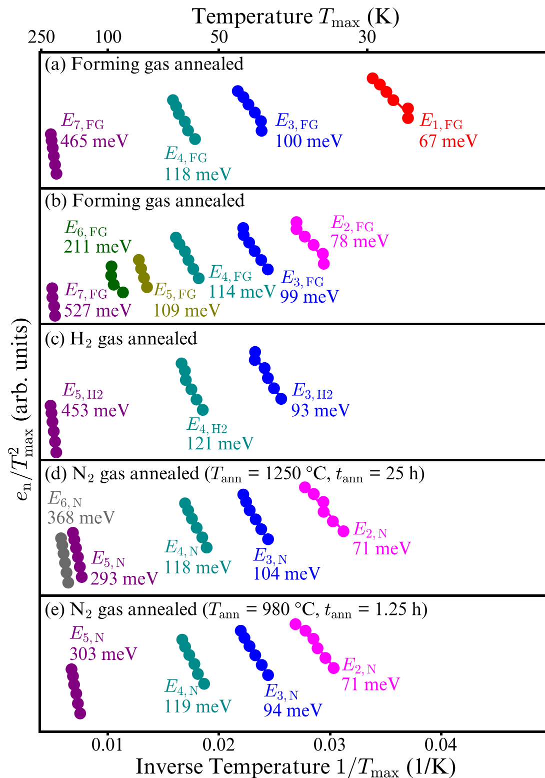

FIG. 6. Arrhenius plots according to Eq. (4) derived from the DLTS measurements shown in Fig. 5.

The interpretation of TAS and DLTS data is facilitated by uniform net carrier concentration versus depth profiles acquired at high measurement frequencies (≥10 kHz). Indeed, this was confirmed for all the samples presented here prior to TAS and/or DLTS measurements. The validity of the TAS and DLTS analysis is furthermore corroborated by the applicability of Eqs. (2) and (4). For essentially all the observed defect levels, an Arrhenius dependence holds for the extracted electron emission rates. The exception is the shallow level $D_{1,FG}$, which is affected by charge carrier freeze-out.

B. Origin of the observed defect levels

The data in Figs. 3–6 reveal the presence of some rather prominent shallow electron traps ($E_A \leq 130$ meV) and that charge carrier-freeze out is limited even at 28 K. Irrespective of the sample production batch and the post-growth heat treatment employed, three particular levels always occur. They exhibit similar electron emission rates as a function of temperature in each sample with $E_A \approx 70$ meV ($D_{3,FG}$, $E_{2,FG}$, $D_{1,H2}$, $D_{2,N}$, and $E_{2,N}$), $E_A \approx 95$ meV ($E_{3,FG}$, $D_{2,H2}$, $E_{3,H2}$, and $E_{2,N}$), and $E_A \approx 120$ meV ($E_{4,FG}$, $D_{3,H2}$, and $E_{4,N}$), respectively. This implies that these levels arise from intrinsic defects or defects involving omnipresent residual impurities. Generally, the absolute concentrations of defect levels in TiO_2 are difficult to determine with a high degree of accuracy because of the uncertainty in the dielectric constant (permittivity).[10–12,55,56] However, by assuming $\epsilon_r = 100$ (as for the CV data), one arrives at values of 10^{15}–10^{17} cm^{-3} for most of the levels in Fig. 5.

Polaronic effects are strong in rutile TiO_2 and may be responsible for some of the observed levels via self-trapping of electrons on Ti sites. For instance, Frederikse[61] and Deák *et al.*,[24] as well as Janotti *et al.*,[23] have reported experimental and theoretical indications, respectively, of such electron states with E_A below 150 meV. Other prevalent intrinsic candidates anticipated in reduced rutile TiO_2 are the donor-like Ti_i and V_O centers.[6,16,17,19] However, reports on the E_A values for these two centers are scarce in the literature. Brandão *et al.*[14] suggested $E_A \approx 2.8$ meV for a V_O donor-state based on electron paramagnetic resonance measurements, which is considerably lower than the thermal activation energy of our three "general" levels. On the other hand, rather recent

density functional theory (DFT) calculations by Janotti *et al.*[23] predict single and double donor states of V_O with E_A equal to about 100 meV and 140 meV, respectively, for a configuration where the donor electrons are rather localized at neighboring Ti atoms ($V_O^{+2} + 2Ti^{+3}$). Hence, V_O cannot be excluded as the origin of our 95 meV and 120 meV levels. Furthermore, Deák *et al.*[24] computed $E_A \approx 100$ meV and $\approx$1300 meV for the single and double donor states, respectively, of a V_O configuration where the electrons are localized at the V_O site. Mattioli *et al.*[37] conducted similar calculations as in Ref. 24 but found a substantially lower E_A value of about 300 meV for the double donor state. For thermally induced charge state transitions of Ti_i in rutile TiO_2, Hubbard-U corrected DFT data by Mattioli *et al.*[37] suggest that the single and double donor levels are resonant with the conduction band, whilst the triple and quadruple ones are located in the bandgap at $\approx$70 meV and 400 meV below the conduction band edge. Thus, Ti_i may be an intrinsic candidate for the common level observed at 70 meV in our samples.

Main residual impurities found in all the investigated samples are H, Li, Al, Si, and Cr according to FTIR and SIMS measurements. Li displays a concentration below 10^{16} cm^{-3}, and the three latter ones exhibit concentrations between 10^{16} and 10^{17} cm^{-3}. The H content is estimated to increase from the 10^{16} cm^{-3} range in the as-received samples to above 10^{18} cm^{-3} after the forming gas and H_2 gas anneals where the absorption signal saturates. Si substitutes for Ti in rutile TiO_2[71,72] and is not expected to introduce localized electronic states in the bandgap but rather to give rise to bandgap narrowing.[60,72] Li in an interstitial configuration is potentially a shallow donor,[26,60] but the predicted E_A value is only 30 meV and does not agree with those of our three common levels. Also, the anticipated electron trap positions associated with Cr in rutile TiO_2 deviate substantially from those of our three common levels, exhibiting values of 190 meV and 410 meV below the conduction band edge.[46] Hence, both Li and Cr (as well as Si) are ruled out as likely candidates for the three common levels while Al in combination with V_O appears to be a more plausible suggestion. Al itself substitutes for Ti and gives rise to an acceptor level in the lower part of the bandgap, i.e., Al on the Ti site acts as a p-type dopant.[34,73] However, on the basis of generation noise recombination and temperature-dependent Hall effect measurements, it is argued by different authors[60,74] that Al-related shallow acceptor states also occur close to the conduction band. In particular, Acket and Volger[60] have ascribed a level at $\sim$50 meV below the conduction band edge to a $2Al_{Ti}$ -V_O complex which may be associated with our most shallow "general" defect level ($E_A \approx 70$ meV) or alternatively with the prominent one at $\approx$60 meV detected after forming gas and N_2 gas anneals only ($D_{2,FG}$, $D_{2,N}$).

Interstitial H is prevailing in all the studied samples, as manifested by its characteristic absorption line at $\sim$3290 cm^{-1} in the acquired IR spectra. This holds already for the as-received samples and becomes even more clear after the forming gas and H_2 gas heat treatments. H_i is a shallow donor in TiO_2, and the 3290 cm^{-1} line originates from the local vibrational mode of an O-H bond oriented perpendicular to the c-axis of the crystal.[30,53] Monitoring the free carrier absorption as a function of temperature and concurrently the transformation between neutral and positively ionized H_i, Herklotz *et al.*[30] determined E_A to be 10 ± 1 meV for the H_i donor. This value is also corroborated by a muon spectroscopy study conducted by Shimomura *et al.*[22] To the best of our knowledge, no corresponding theoretical estimates are available in the literature. Accordingly, H_i can be excluded as the origin of any of the three "general" defect levels observed in the present samples. However, in addition to Ti_i and possibly V_O, H_i is an obvious candidate for the strong shallow donor activity found in our samples, exhibiting limited carrier freeze-out even at 28 K. That is, the dominant donor(s) must have an ionization energy below $\sim$25 meV. Such very shallow donor states in reduced rutile TiO_2 have also been reported by other authors,[9–13] and they are, indeed, expected to be due to intrinsic defect defects (like Ti_i and possibly V_O) and/or common residual impurities (like H_i). Here, it should also be noted that the abnormal decrease in the depletion capacitance observed at temperatures above 50–100 K in the TAS measurements (Fig. 3) is not caused by a decreasing concentration of ionized shallow donors but primarily attributed to the temperature variation of ϵ_r in rutile TiO_2.[55]

Finally, as demonstrated in Fig. 5, no common deep-level defect ($E_A \geq 200$ meV) is found to be present in different samples. A rather prominent level with $E_A \approx 300$ meV exists after N_2 gas annealing ($E_{5,N}$) but not after forming gas and H_2 gas annealing. The opposite holds for the pronounced level with $E_A \approx 460$ meV ($E_{7,FG}$ and $E_{5,H2}$), present after forming gas and H_2 gas annealing but not after N_2 gas annealing. This indicates that these levels arise from (i) defects involving residual impurities with varying concentrations in different samples and/or (ii) complexes involving intrinsic defects being strongly influenced by the annealing conditions used. Further work needs to be pursued in order to resolve this issue.

V. SUMMARY

The DLTS and TAS techniques are demonstrated to be highly applicable for detailed investigations of electrically active defects in rutile TiO_2 single crystals. A comprehensive study of Pd/TiO_2/InGa junctions has been performed using TiO_2 crystals post-growth heat-treated in FG, H_2, or N_2 atmospheres. Irrespective of the sample production batch and the heat-treatment employed, three rather shallow levels occur in all the samples with $E_A \approx 70$ meV, ≈ 95 meV and $\approx$120 meV, respectively. The origins of these levels are discussed in some detail where electron polarons and intrinsic defects such as Ti_i and V_O appear as viable candidates and complexes involving common residual impurities, especially Al in combination with V_O. Furthermore, TAS data display limited charge carrier freeze-out even at 28 K (minimum temperature reached) and evidence the presence of dominant and very shallow donors ($E_A \leq 25$ meV). An obvious shallow donor is the omnipresent H_i, as revealed by infrared absorption measurements of the studied samples, having an ionization energy of only $\sim$10 meV. In contrast to the shallow defects, no common deep-level defect is found to be

present in different samples, possibly indicating a stronger dependence on the annealing conditions used.

ACKNOWLEDGMENTS

Financial support by the Faculty of Mathematics and Natural Sciences at the University of Oslo via the strategic research initiative FOXHOUND and the Research Council of Norway via the EEA-JRP-RO-NO-2013-1 European Project (PERPHECT) is gratefully acknowledged. Experimental support by the Norwegian Micro- and Nano-fabrication facility (NorFab) is highly appreciated.

[1]A. Fujishima and K. Honda, Nature **213**, 8656 (1972).
[2]O. Carp, C. L. Huisman, and A. Reller, Prog. Solid State Chem. **32**, 33 (2004).
[3]Y. Cong, J. Zhang, F. Chen, and M. Anpo, J. Phys. Chem. C **111**, 6976 (2007).
[4]M. Grätzel, Inorg. Chem. **44**, 6841 (2005).
[5]A. Kojima, K. Teshima, Y. Shirai, and T. Miyasaka, J. Am. Chem. Soc. **131**, 6050 (2009).
[6]X. Pan, M.-Q. Yang, X. Fu, N. Zhang, and Y.-J. Xu, Nanoscale **5**, 3601 (2013).
[7]A. Naldoni, M. Allieta, S. Santangelo, M. Marelli, F. Fabbri, S. Cappelli, C. L. Bianchi, R. Psaro, and V. Dal Santo, J. Am. Chem. Soc. **134**, 7600 (2012).
[8]Z. Wang, C. Yang, T. Lin, H. Yin, P. Chen, D. Wan, F. Xu, F. Huang, J. Lin, X. Xie, and M. Jiang, Adv. Funct. Mater. **23**, 5444 (2013).
[9]P. F. Chester and D. H. Bradhurst, Nature **199**, 1056 (1963).
[10]R. G. Breckenridge and W. R. Hosler, Phys. Rev. **91**, 793 (1953).
[11]J. W. Deford and O. W. Johnson, J. Appl. Phys. **54**, 889 (1983).
[12]F. A. Grant, Rev. Mod. Phys. **31**, 646 (1959).
[13]J. H. Becker and W. R. Hosler, Phys. Rev. **137**, A1872 (1965).
[14]F. D. Brandão, M. V. B. Pinheiro, G. M. Ribeiro, and K. Krambrock, Phys. Rev. B **80**, 235204 (2009).
[15]M. K. Nowotny, T. Bak, and J. Nowotny, J. Phys. Chem. B **110**, 16270 (2006).
[16]M. K. Nowotny, L. R. Sheppard, T. Bak, and J. Nowotny, J. Phys. Chem. C **112**, 5275 (2008).
[17]T. Bak, J. Nowotny, M. Rekas, and C. C. Sorrell, J. Phys. Chem. Solids **64**, 1057 (2003).
[18]W. D. Ohlsen and O. W. Johnson, J. Appl. Phys. **44**, 1927 (1973).
[19]P. Deák, B. Aradi, and T. Frauenheim, Phys. Rev. B **92**, 045204 (2015).
[20]C. G. Van de Walle and J. Neugebauer, J. Appl. Phys. **95**, 3851 (2004).
[21]R. Vilão, R. Vieira, H. Alberto, J. Gil, A. Weidinger, R. Lichti, B. Baker, P. Mengyan, and J. Lord, Phys. Rev. B **92**, 081202 (2015).
[22]K. Shimomura, R. Kadono, A. Koda, K. Nishiyama, and M. Mihara, Phys. Rev. B **92**, 075203 (2015).
[23]A. Janotti, C. Franchini, J. B. Varley, G. Kresse, and C. G. Van de Walle, Phys. Status Solidi - RRL **7**, 199 (2013).
[24]P. Deák, B. Aradi, and T. Frauenheim, Phys. Rev. B **86**, 195206 (2012).
[25]A. T. Brant, N. C. Giles, and L. E. Halliburton, J. Appl. Phys. **110**, 53714 (2011).
[26]A. T. Brant, N. C. Giles, L. E. Halliburton, A. T. Brant, N. C. Giles, and L. E. Halliburton, J. Appl. Phys. **113**, 053712 (2013).
[27]V. N. Bogomolov, Y. A. Firsov, E. K. Kudinov, and D. N. Mirlin, Phys. Status Solidi B **35**, 555 (1969).
[28]V. N. Bogomolov and D. N. Mirlin, Phys. Status Solidi B **27**, 443 (1968).
[29]A. Hupfer, L. Vines, E. V. Monakhov, B. G. Svensson, and F. Herklotz, Phys. Rev. B **96**, 085203 (2017).
[30]F. Herklotz, E. V. Lavrov, and J. Weber, Phys. Rev. B **83**, 235202 (2011).
[31]W. P. Chen, Y. Wang, and H. L. W. Chan, Appl. Phys. Lett. **92**, 112907 (2008).
[32]L.-B. Mo, Y. Wang, Y. Bai, Q.-Y. Xiang, Q. Li, W.-Q. Yao, J.-O. Wang, K. Ibrahim, H.-H. Wang, C.-H. Wan *et al.*, Sci. Rep. **5**, 17634 (2015).
[33]D. C. Cronemeyer, Phys. Rev. **113**, 1222 (1959).
[34]E. Yagi, R. Hasiguti, and M. Aono, Phys. Rev. B **54**, 7945 (1996).
[35]C. N. Duckworth, A. W. Brinkman, and J. Woods, Phys. Status Solidi A **75**, K99 (1983).
[36]K. Kobayashi, M. Takata, Y. Fujimura, and S. Okamoto, J. Appl. Phys. **60**, 4191 (1986).
[37]G. Mattioli, P. Alippi, F. Filippone, R. Caminiti, and A. A. Bonapasta, J. Phys. Chem. C **114**, 21694 (2010).
[38]G. Mattioli, F. Filippone, P. Alippi, and A. A. Bonapasta, Phys. Rev. B **78**, 241201(R) (2008).
[39]H. Iddir, Ö. Serdar, P. Zapol, and N. D. Browning, Phys. Rev. B **75**, 073203 (2007).
[40]J. He, R. K. Behera, M. W. Finnis, X. Li, E. C. Dickey, S. R. Phillpot, and S. B. Sinnott, Acta Mater. **55**, 4325 (2007).
[41]D. L. Losee, J. Appl. Phys. **46**, 2204 (1975).
[42]J. Pautrat, B. Katircioglu, N. Magnea, D. Bensahel, J. Pfister, and L. Revoil, Solid-State Electron. **23**, 1159 (1980).
[43]D. V. Lang, J. Appl. Phys. **45**, 3023 (1974).
[44]S. A. Rabie, Phys. Rev. B **14**, 2569 (1976).
[45]R. R. Addiss, A. K. Ghosh, and F. G. Wakim, Appl. Phys. Lett. **12**, 397 (1968).
[46]R. W. A. Hillhouse, "The optical and electrical properties of titanium dioxide," Ph.D. thesis (Durham University, 1981).
[47]M. B. Farah, J. Electrochem. Soc. **145**, 3550 (1998).
[48]J. Bonkerud, C. Zimmermann, F. Herklotz, E. Monakhov, L. Vines, and B. G. Svensson, "Electrical Characteristics of Pd Schottky Diodes on Hydrogenated TiO_2" (unpublished).
[49]R. Schifano, E. V. Monakhov, U. Grossner, and B. G. Svensson, Appl. Phys. Lett. **91**, 193507 (2007).
[50]B. G. Svensson, K. H. Rydén, and B. M. S. Lewerentz, J. Appl. Phys. **66**, 1699 (1989).
[51]A. A. Istratov, O. F. Vyvenko, H. Hieslmair, and E. R. Weber, Meas. Sci. Technol. **9**, 477 (1998).
[52]R. Schifano, E. V. Monakhov, B. G. Svensson, W. Mtangi, P. Janse van Rensburg, and F. D. Auret, Phys. B: Condens. Matter **404**, 4344 (2009).
[53]O. W. Johnson, J. Deford, and J. W. Shaner, J. Appl. Phys. **44**, 3008 (1973).
[54]P. Blood and J. W. Orton, *The Electrical Characterization of Semiconductors: Majority Carriers and Electron States* (Academic Press, 1992), Vol. 13.
[55]R. A. Parker, Phys. Rev. **124**, 1719 (1961).
[56]J. Li, F. Li, X. Zhu, D. Lin, Q. Li, W. Liu, and Z. Xu, J. Alloys Compd. **692**, 375 (2017).
[57]K. J. Yang and C. Hu, IEEE Trans. Electron Devices **46**, 1500 (1999).
[58]T. P. Weiss, A. Redinger, D. Regesch, M. Mousel, and S. Siebentritt, IEEE J. Photovoltaics **4**, 1665 (2014).
[59]J. Pascual, J. Camassel, and H. Mathieu, Phys. Rev. B **18**, 5606 (1978).
[60]G. Acket and J. Volger, Physica **32**, 1680 (1966).
[61]H. P. R. Frederikse, J. Appl. Phys. **32**, 2211 (1961).
[62]V. Cristea and V. Babeş, Phys. Status Solidi A **45**, 617 (1978).
[63]W. R. Thurber and A. J. H. Mante, Phys. Rev. **139**, A1655 (1965).
[64]J. F. Baumard and F. Gervais, Phys. Rev. B **15**, 2316 (1977).
[65]S. Chakraborty, M. K. Bera, P. K. Bose, and C. K. Maiti, Semicond. Sci. Technol. **21**, 335 (2006).
[66]L. A. Harris and R. Schumacher, J. Electrochem. Soc. **127**, 1186 (1980).
[67]T. Minato, Y. Sainoo, Y. Kim, H. S. Kato, K.-i. Aika, M. Kawai, J. Zhao, H. Petek, T. Huang, W. He, and B. Wang, J. Chem. Phys. **130**, 124502 (2009).
[68]G. I. Roberts and C. R. Crowell, J. Appl. Phys. **41**, 1767 (1970).
[69]J. D. Wiley and G. L. Miller, IEEE Trans. Electron Devices **22**, 265 (1975).
[70]A. Broniatowski, A. Blosse, P. C. Srivastava, and J. C. Bourgoin, J. Appl. Phys. **54**, 2907 (1983).
[71]S. Yang, L. E. Halliburton, A. Manivannan, P. H. Bunton, and D. B. Baker, Appl. Phys. Lett. **94**, 162114 (2009).
[72]K. Yang, Y. Dai, and B. Huang, Chem. Phys. Lett. **456**, 71 (2008).
[73]J. Yahia, Phys. Rev. **130**, 1711 (1963).
[74]R. Zijlstra, F. Leeuwerik, and T. Kleinpenning, Phys. Lett. **23**, 185 (1966).